

## Article

# Materials Based on Co, Cu, and Cr as Activators of PMS for Degrading a Representative Antibiotic—The Strategy for Utilization in Water Treatment and Warnings on Metal Leaching

Efraím A. Serna-Galvis <sup>1,2,\*</sup>, Carlos Mendoza-Merlano <sup>2</sup> , Ricardo A. Torres-Palma <sup>1</sup> , Adriana Echavarría-Isaza <sup>2</sup> and Dora A. Hoyos-Ayala <sup>3,\*</sup>

<sup>1</sup> Grupo de Investigación en Remediación Ambiental y Biocatálisis (GIRAB), Instituto de Química, Facultad de Ciencias Exactas y Naturales, Universidad de Antioquia UdeA, Medellín 050010, Colombia; ricardo.torres@udea.edu.co

<sup>2</sup> Grupo de Catalizadores y Adsorbentes (CATALAD), Instituto de Química, Facultad de Ciencias Exactas y Naturales, Universidad de Antioquia UdeA, Medellín 050010, Colombia; cjavier.mendoza@udea.edu.co (C.M.-M.); adriana.echavarría@udea.edu.co (A.E.-I.)

<sup>3</sup> Grupo de Ingeniería y Gestión Ambiental (GIGA), Facultad de Ingeniería, Universidad de Antioquia UdeA, Medellín 050010, Colombia

\* Correspondence: efrain.serna@udea.edu.co (E.A.S.-G.); dora.hoyos@udea.edu.co (D.A.H.-A.)

**Abstract:** A chromate of copper and cobalt ( $\Phi$ y) was synthesized and characterized.  $\Phi$ y activated peroxymonosulfate (PMS) to degrade ciprofloxacin (CIP) in water. The  $\Phi$ y/PMS combination showed a high degrading capability toward CIP (~100% elimination in 15 min). However,  $\Phi$ y leached cobalt ( $1.6 \text{ mg L}^{-1}$ ), limiting its use for water treatment. To avoid leaching,  $\Phi$ y was calcinated, forming a mixed metal oxide (MMO). In the combination of MMO/PMS, no metals leached, the CIP adsorption was low (<20%), and the action of  $\text{SO}_4^{\bullet-}$  dominated, leading to a synergistic effect on pollutant elimination (>95% after 15 min of treatment). MMO/PMS promoted the opening and oxidation of the piperazyl ring, plus the hydroxylation of the quinolone moiety on CIP, which potentially decreased the biological activity. After three reuse cycles, the MMO still presented with a high activation of PMS toward CIP degradation (90% in 15 min of action). Additionally, the CIP degradation by the MMO/PMS system in simulated hospital wastewater was close to that obtained in distilled water. This work provides relevant information on the stability of Co-, Cu-, and Cr-based materials under interaction with PMS and the strategies to obtain a proper catalyst to degrade CIP.

**Keywords:** ciprofloxacin degradation; chromate of copper and cobalt; PMS activation; metal leaching; mixed metal oxides; water treatment



**Citation:** Serna-Galvis, E.A.; Mendoza-Merlano, C.; Torres-Palma, R.A.; Echavarría-Isaza, A.; Hoyos-Ayala, D.A. Materials Based on Co, Cu, and Cr as Activators of PMS for Degrading a Representative Antibiotic—The Strategy for Utilization in Water Treatment and Warnings on Metal Leaching.

*Molecules* **2023**, *28*, 4536. <https://doi.org/10.3390/molecules28114536>

Academic Editors: Isidro M. Pastor, Luísa Margarida Martins and Maria Luisa Di Gioia

Received: 29 April 2023

Revised: 27 May 2023

Accepted: 30 May 2023

Published: 3 June 2023



**Copyright:** © 2023 by the authors. Licensee MDPI, Basel, Switzerland. This article is an open access article distributed under the terms and conditions of the Creative Commons Attribution (CC BY) license (<https://creativecommons.org/licenses/by/4.0/>).

## 1. Introduction

Antibiotics are pharmaceuticals that are used worldwide to prevent and treat infections in humans and animals. The overuse of antibiotics in hospitals, agriculture, and livestock activities is promoting the development of antibiotic-resistant bacteria, which represents global environmental and health concerns [1,2]. Currently, effluents from hospital wastewater are considered a concerning source of releasing antibiotics into the environment [3,4]. Most of the antibiotics are recalcitrant to conventional water treatments [5]. Thus, the application of alternative processes able to eliminate antibiotics is urgently needed.

Advanced oxidation processes (AOPs) are alternatives that take advantage of short-lived and highly reactive oxygen species (ROS, e.g.,  $\text{HO}^{\bullet}$ ), which have been successfully utilized for the abatement of organic pollutants [6]. Typical AOPs, such as Fenton- and UV-based processes, generate ROS by activating hydrogen peroxide. Recently, AOPs utilizing peroxymonosulfate (PMS) or peroxydisulfate (PDS) (collectively referred to as persulfate-based AOPs) instead of hydrogen peroxide have emerged as an option to produce ROS

and reactive sulfate species (RSS, e.g.,  $\text{SO}_4^{\bullet-}$ ) to deal with organic pollutants in aqueous samples [7].

Among persulfate-based AOPs, the catalytic activation of PMS is a field of increasing interest in the scientific community because this kind of process allows the use of diverse homogeneous (such as  $\text{Fe}^{2+}$  or  $\text{Co}^{2+}$  in solution) or heterogeneous (such as transition metal oxides, activated carbons, biochars, or reduced graphene oxides) catalysts to easily promote the formation of ROS and RSS for degrading a wide variety of contaminants [7,8].

Cobalt is a key element in the heterogeneous catalytic activation of PMS. Cobalt-containing catalysts can be designed with a peculiar morphology or structure in order to enhance the efficiency of persulfate activation toward the production of ROS and RSS. In the heterogeneous catalytic activation of peroxides, it is also very common to utilize solids containing other transition metals, in addition to cobalt [9,10]. For instance, chromate species have been used to activate hydrogen peroxide for degrading organic pollutants in water [11]. Recently, chromium-substituted magnetite nanoparticles, or recycled chromium phosphate as a support of cobalt oxide, have been tested in the activation of PMS to deal with water contaminants [12,13]. However, to the best authors' knowledge, still, the use of chromates of copper and cobalt and their corresponding oxides to activate PMS for the elimination of organic pollutants has not yet been reported.

In this work, chromate of cobalt and copper ( $\Phi_y$ ) and its corresponding mixed metal oxide (MMO, coming from  $\Phi_y$  calcination) were prepared and used in a catalytic AOP. The catalysts' stability (metals leaching and reuse) and the risk of releasing heavy metals from the catalysts into the solution were discussed. Both  $\Phi_y$  and MMO were characterized and tested as activators of PMS for degrading a representative contaminant of emerging concern (i.e., ciprofloxacin, CIP).  $\Phi_y$  was synthesized using a hydrothermal method. Once  $\Phi_y$  was prepared and characterized, its activating ability was assessed, and the results suggested that the  $\Phi_y$ /PMS system quickly degraded CIP. However, PMS promoted the dissolution of cobalt from the solid material, changing the system from a heterogeneous to a homogeneous catalysis. Considering the issues associated with metal leaching,  $\Phi_y$  was calcinated to produce MMO. Then, the activation of PMS by MMO, activation pathways, and primary transformations were established. The change in the biological activity of CIP by the treatment was studied using theoretical analyses. Moreover, the treatment extent, testing the reuse cycles of the catalyst and the degradation of CIP in simulated hospital wastewater with the MMO/PMS system, was assessed. In the PMS/MMO process, the radical route dominated the target pollutant degradation and promoted the opening and the oxidation of the piperazyl ring and the hydroxylation of the quinolone moiety on CIP. The process presented high activation of PMS toward CIP degradation and the capability to change the biological activity of the antibiotic. After three reuse cycles, the MMO was still active toward PMS for the CIP degradation. Additionally, the CIP degradation in the simulated hospital wastewater was close to that obtained in distilled water.

## 2. Results and Discussion

### 2.1. Characterization of the $\Phi_y$

The chromate of copper and cobalt was synthesized by using the hydrothermal method and it was characterized using atomic absorption (composition), X-ray diffraction (XRD), Brunauer–Emmett–Teller analysis (BET), thermogravimetric analysis (TGA), and scanning electron microscopy (SEM). Figure 1a presents the XRD pattern of the synthesized material. This pattern shows a perfect correlation with the chromate phase  $\Phi_y$  (corresponding to  $(\text{NH}_4)_{1.5}\text{Co}_x\text{Cu}_{2-x}\text{Cr}_2\text{O}_8(\text{OH})_{1.5}\cdot\text{H}_2\text{O}$ , [14]) according to the ICSD database 98-009-3960. Table 1 summarizes the composition and the BET results. The content of Cu, Cr, and Co (which are relevant metals for the PMS activation) in  $\Phi_y$  was at 28.3, 5.87, and 9.39% *w/w*, respectively. From the TGA analysis (Figure 1b), it was observed that, between 100 and 300 °C, there was an 18% loss of weight, due to the release of water and ammonium. The second event between 400 and 500 °C and the third event between 850 and 900 °C, having a 3.9% and 5.3% loss of weight, respectively, were due to oxygen desorption. In turn,

the textural results presented in Table 1 indicate that half of the BET area mainly comes from the mesopore, which is associated with the external interparticle, and the rest of the area comes from the micropore interlaminar space. Additionally, the high total pore volume, calculated at  $p/p_0 = 0.995$ , is mainly due to the high  $N_2$  uptake characteristic of nanometric-sized particles. In turn, Figure 1c (SEM micrograph) shows that the  $\Phi y$  material has particles with laminar morphology (flake-shaped particles), also supporting the textural analysis determined by  $N_2$  physisorption, with very well-defined crystals and with a lamellar extension that reaches up to microns.

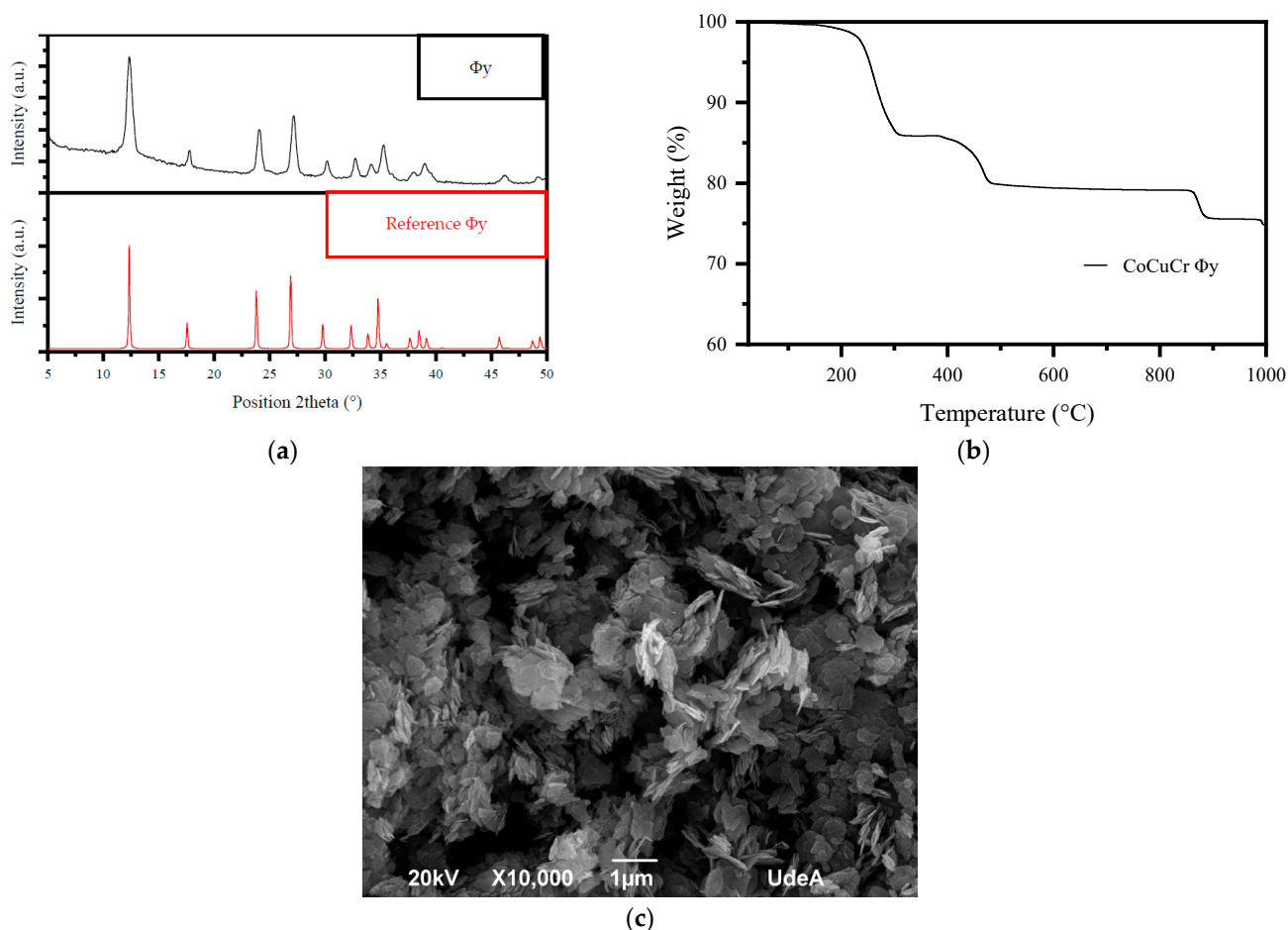


**Figure 1.** Characterization of chromate of copper and cobalt ( $\Phi y$ ). (a) XRD pattern of  $\Phi y$ . (b) TGA for  $\Phi y$ . (c) SEM for  $\Phi y$ .

**Table 1.** Elemental composition and BET results for  $\Phi y$ .

Sample	Metals * (%w/w)			
	Cu	Cr	Co	
$\Phi y$	28.30	5.87	9.39	
Property	$V_{\text{micro}}$ ( $\text{cm}^3 \text{g}^{-1}$ )	$V_{\text{total}}$ ( $\text{cm}^3 \text{g}^{-1}$ )	$S_{\text{BET}}$ ( $\text{m}^2 \text{g}^{-1}$ )	$S_{\text{ext}}$ ( $\text{m}^2 \text{g}^{-1}$ )
Value	0.01	0.203	38.2	18.0

\* Metals determined by AA,  $S_{\text{BET}}$ : surface area BET,  $S_{\text{ext}}$ : external surface area,  $V_{\text{micro}}$ : volume of micropore, and  $V_{\text{total}}$ : total volume.

## 2.2. Activation of PMS for the CIP Degradation

Initially, the adsorption of CIP on the  $\Phi y$  material and the direct oxidation by PMS were tested (Figure 2a). The  $\Phi y$  material alone showed a low adsorption capability toward

the antibiotic (less than 20% of removal at 15 min), due to the low surface area ( $S_{BET}$ :  $38.2 \text{ m}^2 \text{ g}^{-1}$ ) and the low pore volume ( $V_{total}$ :  $0.203 \text{ cm}^3 \text{ g}^{-1}$ ) of this material (Table 1). In turn, the PMS degraded the probe pollutant to some extent ( $\sim 15\%$  after 15 min of interaction). This inorganic peroxide presents a high redox potential ( $E^\circ$ :  $1.82 \text{ V}$ , [15]) and can directly oxidize CIP, thus leading to a decrease in the concentration of the antibiotic (Figure 2a). Interestingly, the combination of  $\Phi\gamma$  with the PMS practically degraded the CIP after 3 min of treatment (Figure 2a), indicating the high activating capability of this material for degrading CIP.

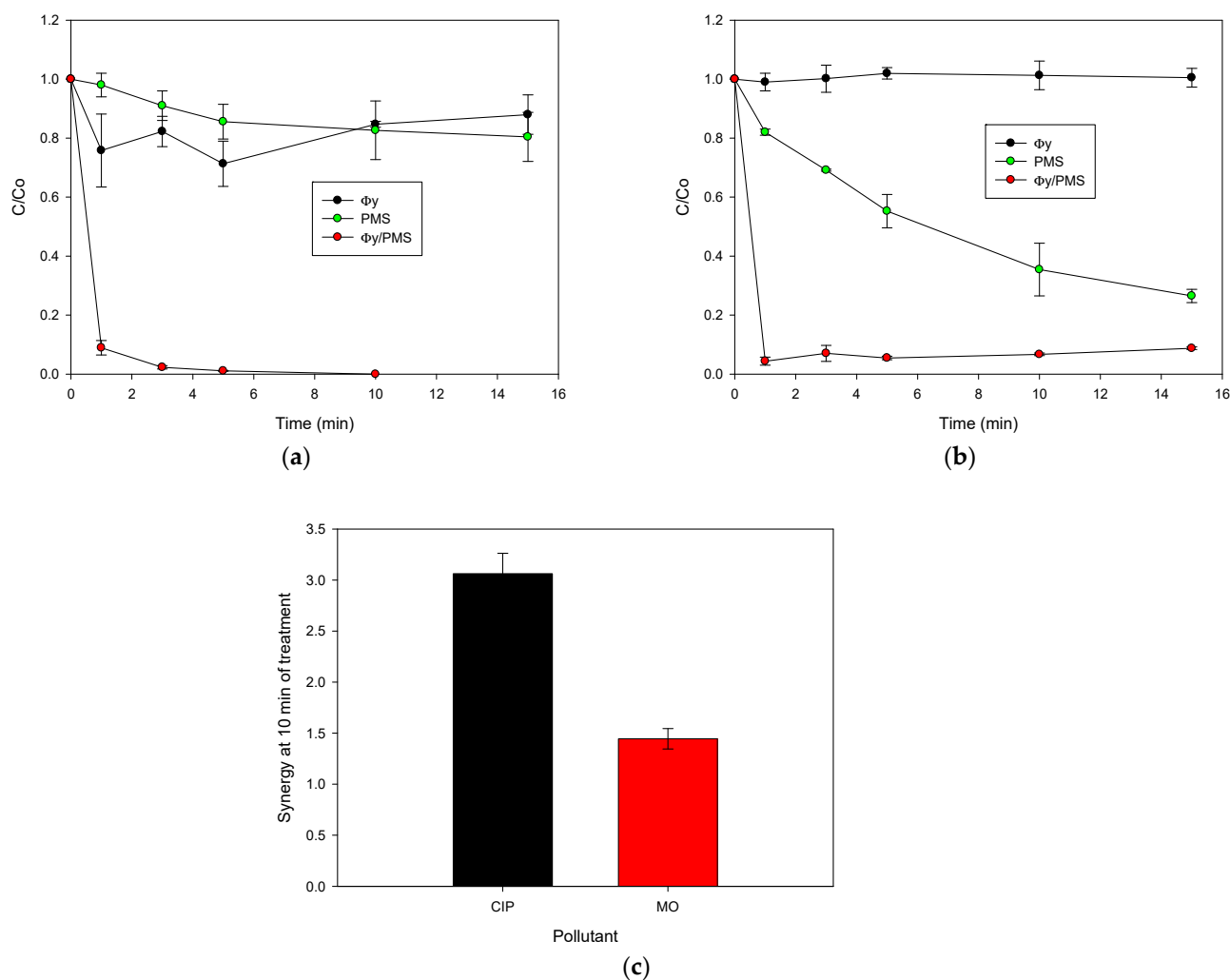


**Figure 2.** Treatment of organic pollutants with the  $\Phi\gamma$ /PMS system. (a) CIP evolution, (b) MO evolution, and (c) synergy in the degradation of CIP and MO. Experimental conditions: CIP =  $30.6 \mu\text{mol L}^{-1}$ , MO =  $30.6 \mu\text{mol L}^{-1}$ ,  $\Phi\gamma$  =  $0.2 \text{ g L}^{-1}$ , PMS =  $500 \mu\text{mol L}^{-1}$ ,  $V$  =  $50 \text{ mL}$ , and initial pH = 5.4.

After testing the ability of  $\Phi\gamma$  to activate the PMS, the  $\Phi\gamma$ /PMS combination was applied in order to treat another organic pollutant, testing the effect of the chemical structure of the contaminant on the process. Therefore, methyl orange (MO) was considered. The structural core of CIP is a quinolone system attached to a piperazyl ring, whereas MO has an azo group connecting two aromatic rings [16]. Figure 2b depicts the results of the treatment of MO. It can be noted that, after 10 min of treatment, the MO pollutant was not adsorbed by  $\Phi\gamma$ . However,  $\sim 70\%$  of the MO was degraded by direct oxidation of the PMS alone. Peroxymonosulfate is a strong oxidant that easily oxidizes MO, which has a lower redox potential ( $E$ :  $\sim 0.96 \text{ V}$  [17]) than PMS. Despite the high degradation of the MO by the PMS alone, the  $\Phi\gamma$ /PMS combination induced more than 90% of the pollutant removal

after only 1 min of treatment, which highlights the high efficiency of the combination ( $\Phi_y$ /PMS).

For the degradation of both pollutants by  $\Phi_y$ /PMS, the synergy was determined (calculated as % removal by the system/ $\Sigma$  and % removal by the individual components of the system) and compared (Figure 2c). The  $\Phi_y$ /PMS system was highly synergistic. Indeed, the synergy values were 3.0 and 1.5 for CIP and MO, respectively, indicating that the enhancement of the degradation of the CIP by using the combined system (i.e.,  $\Phi_y$ /PMS), regarding the individual components ( $\Phi_y$  or PMS), is higher than the improvement obtained for MO. Such enhancements can be associated with the generation and action of the degrading agents from the interaction of PMS with  $\Phi_y$  (e.g., radical species) [7]. This aspect is developed in the following section.

### 2.3. Action Routes of the $\Phi_y$ /PMS System

In order to establish the participation of radicals in the  $\Phi_y$ /PMS process, the treatment of CIP was performed in the presence of methanol (MeOH,  $k_{HO^\bullet}/MeOH$ :  $9.7 \times 10^8 \text{ M}^{-1} \text{ s}^{-1}$ , and  $k_{SO_4^{\bullet-}}/MeOH$ :  $1.0 \times 10^7 \text{ M}^{-1} \text{ s}^{-1}$ , [18]) or tert-butyl alcohol (TBA,  $k_{HO^\bullet}/TBA$ :  $6.0 \times 10^8 \text{ M}^{-1} \text{ s}^{-1}$ , and  $k_{SO_4^{\bullet-}}/TBA$ :  $8.4 \times 10^5 \text{ M}^{-1} \text{ s}^{-1}$ , [18]). These scavengers were used 100-fold more concentrated than the pharmaceutical compound. Moreover, as the CIP degradation by the  $\Phi_y$ /PMS process at  $500 \mu\text{mol L}^{-1}$  of PMS is very fast (Figure 2a), the PMS amount was decreased up to  $100 \mu\text{mol L}^{-1}$  in order to evidence the phenomenon. Figure 3a shows the evolution of the CIP in the absence and presence of the scavengers. MeOH inhibited the pollutant degradation, whereas TBA did not affect the CIP elimination. These results indicated that, in the  $\Phi_y$ /PMS system, the peroxymonosulfate was activated toward the sulfate radical, which is the main species involved in the degradation of CIP. Furthermore, it should also be considered that the  $\Phi_y$  material has copper and chromium elements in their highest oxidation states (2+ and 6+ for Cu and Cr, respectively, according to the XRD and TGA results), limiting the electron transfer (a typical mechanism involved in the activation of peroxymonosulfate [10]). In contrast, the cobalt element is in the oxidation state of 2+, and this metal could transfer an electron, which is very relevant for the activation of PMS [19–21].

As  $\Phi_y$  is a solid material that contains Co, Cu, and Cr, an important aspect to be considered is the release of such metals from the solid into the solution [22]. Therefore, the contribution of homogeneous components in the  $\Phi_y$ /PMS system by the leaching of metal ions was tested. Then, the interaction of the PMS with the solid material in the absence of pollutants was assessed, finding that  $\sim 1.6 \text{ mg L}^{-1}$  of cobalt ions was released from the solid catalyst after 15 min of treatment. In addition, this lixiviate was used to treat CIP (Figure 3b), showing a very fast degradation of the antibiotic. Furthermore, a control experiment using homogeneous cobalt (i.e.,  $\text{Co}^{2+}$  from  $\text{Co}(\text{NO}_3)_2 \times 6\text{H}_2\text{O}$ , at the same concentration lixiviated from  $\Phi_y$ ) was performed (Figure 3b), in which a very fast degradation of the target pollutant was also observed. All of these results evidenced that the homogeneous component has a very strong contribution to the degradation of the pollutants in the  $\Phi_y$ /PMS system.

The addition of PMS to distilled water containing the  $\Phi_y$  material decreased the pH from 5.4 to 3.4. In order to assess the role of a decreasing pH on cobalt ion leaching, other control tests were performed. An experiment evaluating the cobalt release when  $\Phi_y$  is exposed to distilled water at pH 3.4 (adjusted using  $\text{H}_2\text{SO}_4$ ) was carried out, indicating that  $1.6 \text{ mg L}^{-1}$  of cobalt ions were also leached under such conditions. Another control test, which consisted of the addition of  $\Phi_y$  in distilled water containing PMS at pH 5.4 (previously adjusted using NaOH), showed the leaching of  $0.9 \text{ mg L}^{-1}$  of cobalt ions. Additionally, when  $\Phi_y$  was added to distilled water at pH 2.4 (previously adjusted with  $\text{H}_2\text{SO}_4$ , with no presence of PMS), the solid was dissolved quickly and completely. It must be taken into account that, at an acidic pH,  $\text{Co}^{2+}$  predominates in a soluble form, and its redox potential increases according to the typical Pourbaix diagram for this metal [23], which can favor the activation of PMS, and, consequently, a fast elimination of CIP occurs.

Therefore, all of the above results indicate that  $\Phi y$  is not stable during the pH decrease promoted by the PMS addition, thus leading to the release of cobalt ions (Equation (1)) and the promotion of the conversion of the initial heterogeneous system into a homogeneous process. Such a homogeneous system involves the interaction of the released cobalt to produce radical species (Equations (2) and (3), [24,25]), inducing a fast degradation of the target pollutants, as evidenced in Figure 2a,b.

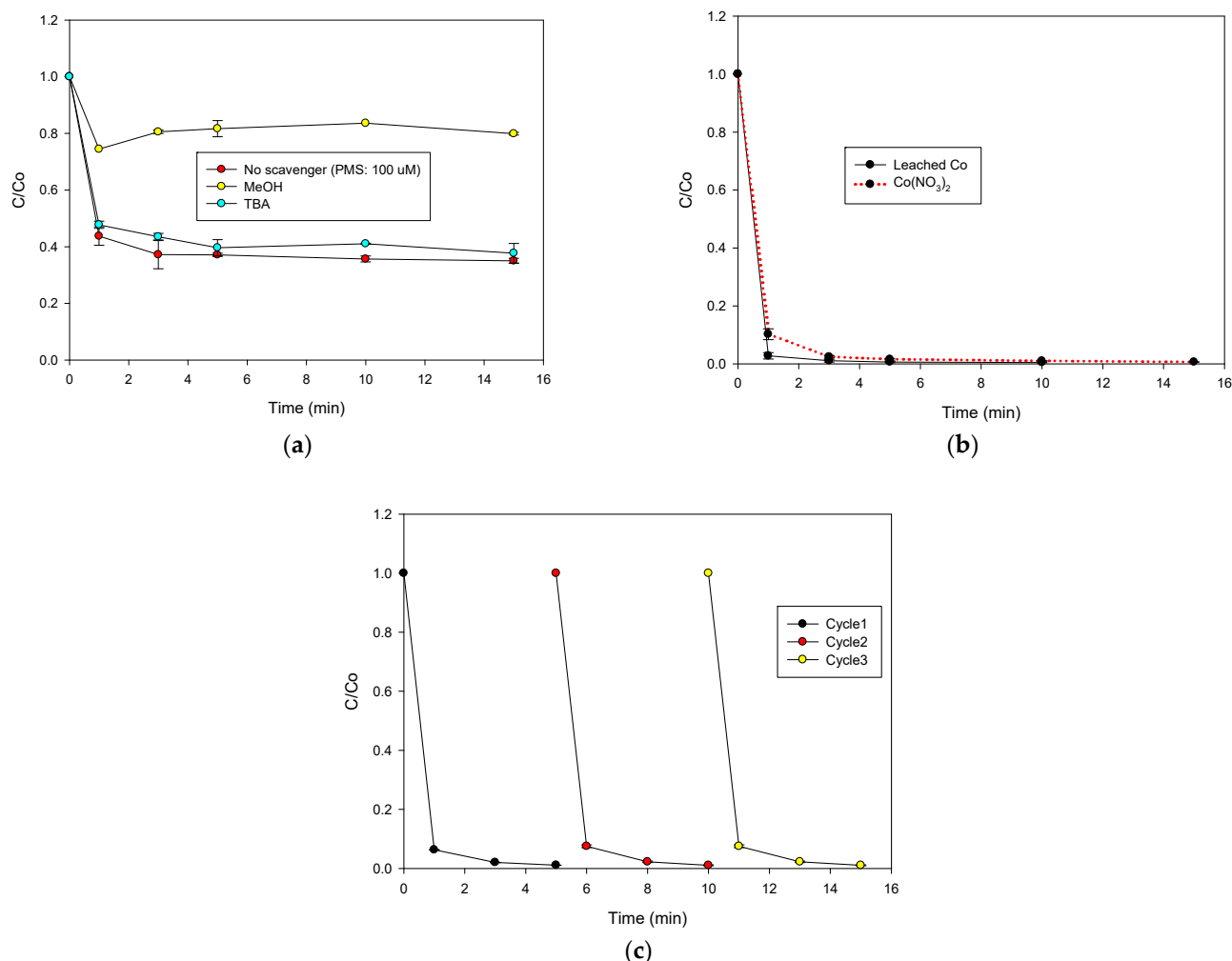
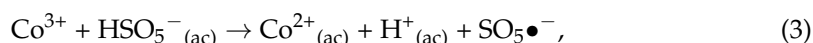
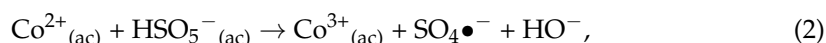


**Figure 3.** Elucidation of degradation routes and reuse cycles of the solid material in the  $\Phi y$ /PMS system. (a) Treatment of CIP in the presence of scavengers, (b) degradation of CIP by leached cobalt or cobalt nitrate, and (c) reuse of  $\Phi y$  in the  $\Phi y$ /PMS system. Experimental conditions: CIP = 30.6  $\mu\text{mol L}^{-1}$ , MeOH = TBA = 3060  $\mu\text{mol L}^{-1}$ ,  $\Phi y$  = 0.2 g  $\text{L}^{-1}$ , PMS = 500  $\mu\text{mol L}^{-1}$  (for (b,c)), V = 50 mL, and initial pH = 5.6.



As the  $\Phi y$  material experiences cobalt leaching, it was very important to assess the activity when it was used for several cycles. Hence, the reusability of  $\Phi y$  was evaluated (Figure 3c). Additionally, the cobalt ions that were released after each cycle were also measured (Table S1, in the Supplementary Materials). It can be noted that, even after the

third reuse cycle,  $\Phi$ y was able to endorse a fast elimination of CIP; however, the amount of leached cobalt ions decreased with each reuse cycle (Table S1). Such results indicate that, even though the leaching of cobalt was diminished after the cycles, the released ions activated PMS, producing enough radical amounts to completely degrade CIP.

It must be noted that, although cobalt ions are very efficient for the homogeneous activation of PMS, water containing such ions has a potential hazard to human health [10]. Even if the maximum permitted emission level for cobalt is low ( $<1.0 \text{ mg L}^{-1}$ ), the long-term operation of leaching materials may induce the accumulation of toxic cobalt in water bodies. Furthermore, the secondary pollution caused by cobalt leaching from the materials during the catalytic activation of PMS should not be overlooked [22]. Indeed, cobalt leaching is a critical point (it is more worrying if cobalt was released at higher concentrations than the maximum permitted emission) that hinders the actual applications of the  $\Phi$ y material for water treatment. Therefore, as a strategy to inhibit cobalt leaching (which is also fairly beneficial for practical uses), the calcination of  $\Phi$ y was applied, generating a mixed metal oxide (MMO). Subsequently, the capability of the MMO to activate the PMS for CIP degradation was tested, as detailed in the following sections.

#### 2.4. PMS Activation Using MMO

As mentioned above, the initial  $\Phi$ y was calcinated at  $450 \text{ }^\circ\text{C}$  (such a calcination temperature was selected to produce the oxide based on the TGA analysis, Figure 1b), producing the MMO material [14]. XRD, BET, SEM, and composition analyses of the MMO were carried out (Figure 4 and Table 2). According to the XRD analyses for the calcinated material and its comparison with the patterns of ICSD 98-008-7126 and ICSD 98-002-7507 (Figure 4a), the MMO is composed of copper oxide (CuO) and cobalt–chromium oxide ( $\text{Co}_x\text{Cu}_{1-x}\text{Cr}_2\text{O}_4$ ), having percentages of 28.5% and 71.5% (which were determined by the Rietveld method ([26], Figure S1), respectively. These aspects evidenced the destruction of the  $\Phi$ y framework and the generation of the mixed metal oxides of Co, Cr, and Cu, which is consistent with our previous work regarding the thermal decomposition of  $\Phi$ y-type materials [14].

**Table 2.** Main properties of the MMO.

Sample	Metals * (%w/w)			
	CuO		$\text{Co}_x\text{Cu}_{1-x}\text{Cr}_2\text{O}_4$	
MMO	28.5		71.5	
Property	$V_{\text{micro.}} (\text{cm}^3 \text{ g}^{-1})$	$V_{\text{total}} (\text{cm}^3 \text{ g}^{-1})$	$S_{\text{BET}} (\text{m}^2 \text{ g}^{-1})$	$S_{\text{ext.}} (\text{m}^2 \text{ g}^{-1})$
Value	0.00	0.230	36.8	36.8

\* Metals determined by AA,  $S_{\text{BET}}$ : surface area BET,  $S_{\text{ext.}}$ : external surface area,  $V_{\text{micro.}}$ : volume of micropore, and  $V_{\text{total}}$ : total volume.

XPS analyses for the MMO were also carried out (Figure 4b). The predominant presence of O and Cr, followed by Cu and Co, can be noted here. This figure also suggests that, in the MMO, the  $\text{Co}_x\text{Cu}_{1-x}\text{Cr}_2\text{O}_4$  component is more exposed on the external surface, while CuO remains more internal. Moreover, from the deconvolution of the XPS peaks (Figure 4c–f), it was found that the surface of the MMO contained species of  $\text{Co}^{2+}$  (44.36%),  $\text{Co}^{3+}$  (55.64%),  $\text{Cu}^+$  (92.32%),  $\text{Cu}^{2+}$  (7.68%),  $\text{Cr}^{3+}$  (~100%), and O (93.62% belonging to the lattice). On the other hand, the  $\text{N}_2$  adsorption on the MMO (Figure S2a) showed an isotherm type IV, with a high  $\text{N}_2$  uptake at the high P/ $P_0$  region, which is typical for materials with interparticle mesoporosity coming from the small particle size. In the absence of micropores, the external surface area provides the main contribution to the total pore volume, and the surface area corresponds to the mesopores among the particles (Table 2) [27]. From Figure S2b, which presents the SEM images for MMO, it can be noted that the calcination of the  $\Phi$ y induced a partial destruction of the flake-shaped particles (Figure 1c). However, the MMO particles inherited some morphological anisotropy from their parent  $\Phi$ y material.

Moreover, the calcination process decreased the size of the particles below 1  $\mu\text{m}$ , generating agglomerates of small particles with elongated shapes (Figure S2b).

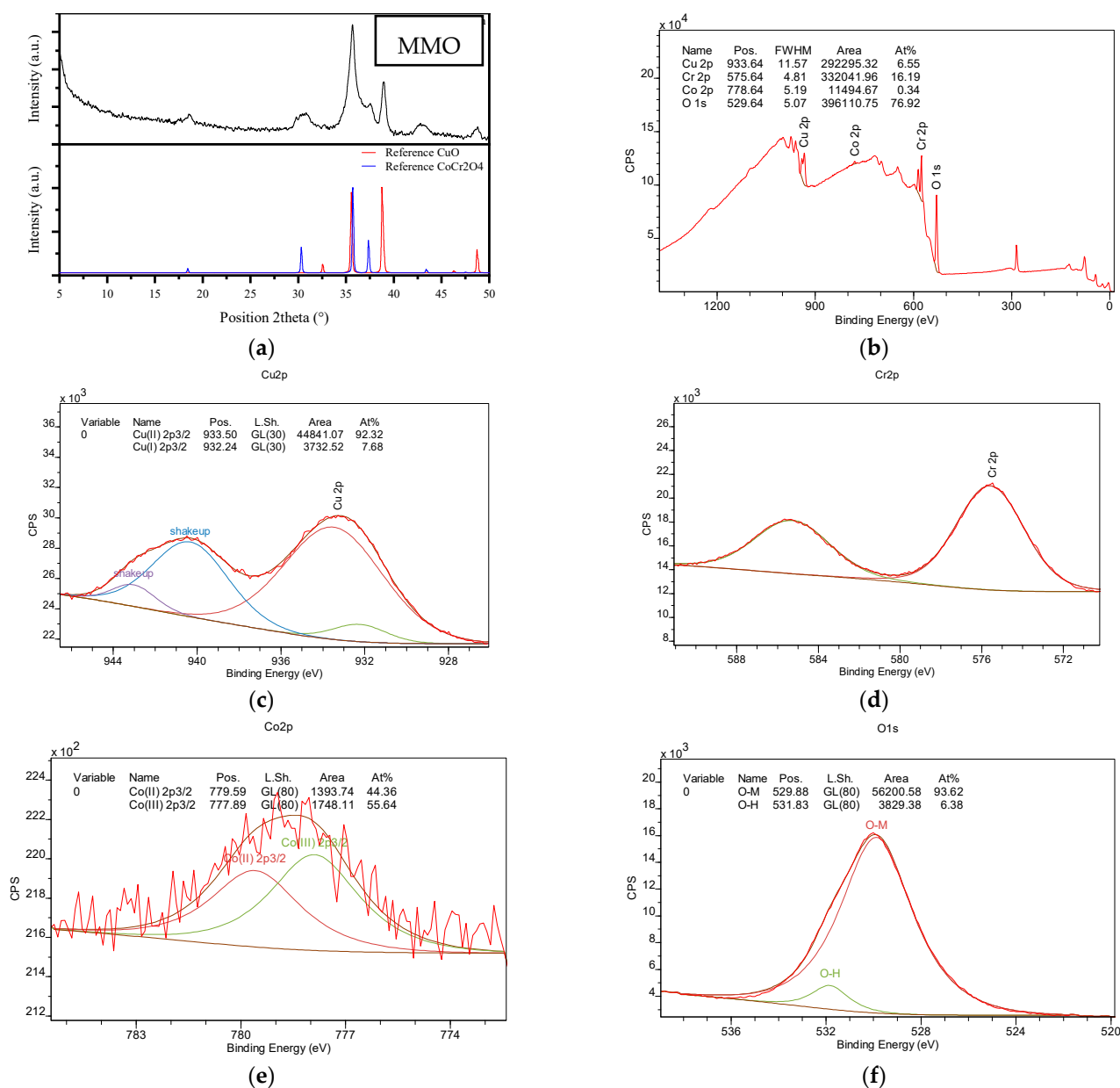


**Figure 4.** Characterization of MMO. (a) XRD, (b) XPS spectrum, (c) deconvolution of the peak for Cu, (d) deconvolution of the peak for Cr, (e) deconvolution of the peak for Co, and (f) deconvolution of the peak for O.

After the characterization of the MMO, its capability for the adsorption and degradation of CIP was tested. Moreover, the leaching of the cobalt ions from the interaction of the MMO with the PMS was also evaluated. Figure 5a shows the adsorption of CIP on the MMO, the direct oxidation by the PMS, and the evolution under the MMO/PMS combination. A low adsorption of CIP on this material was observed (~20% after 15 min of treatment), which is explained by taking into account the low surface area ( $S_{\text{BET}}$ : 36.8 m<sup>2</sup> g<sup>-1</sup>) and pore volume ( $V_{\text{total}}$ : 0.230 cm<sup>3</sup> g<sup>-1</sup>) of the MMO (Table 2). In turn, the MMO/PMS combination led to a CIP elimination that was much higher than that obtained by adsorption or direct oxidation with PMS. Moreover, leaching of cobalt was not detected during the process, indicating a heterogeneous catalytic activation of PMS by the MMO. It is important to note

that MMO has a degradation efficiency similar to that reported for cobalt-doped metal oxide/hydroxide (such as hierarchical Co(II)-doped TiO<sub>2</sub>, cobalt-doped biogenic manganese oxide, or Co-doped Fe<sub>3</sub>O<sub>4</sub>@FeOOH), substrates for heterogeneous PMS activation. However, those substrates have the disadvantage of the Co leaching [22], while MMO does not have this concern.

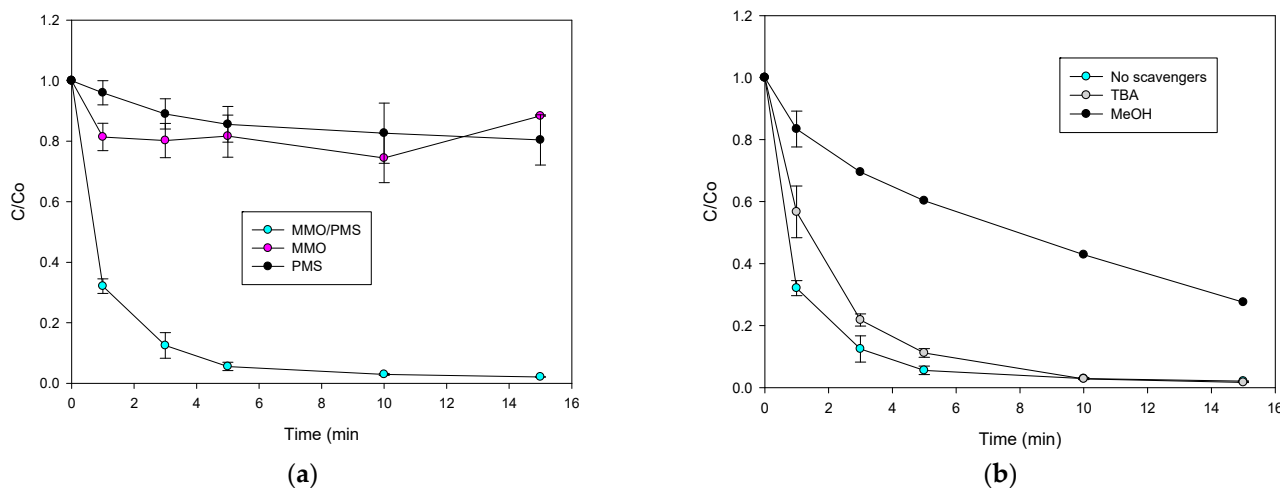
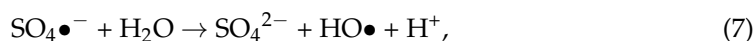
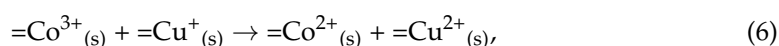
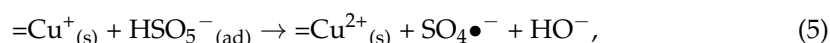
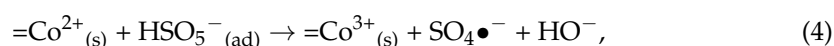


**Figure 5.** Treatment of CIP by the MMO/PMS combination. (a) Degradation of CIP and (b) treatment of CIP in the presence of radical scavengers. Experimental conditions: CIP = 30.6  $\mu\text{mol L}^{-1}$ , MeOH = TBA = 3060  $\mu\text{mol L}^{-1}$  (only for (b)), MMO = 0.2  $\text{g L}^{-1}$ , PMS = 500  $\mu\text{mol L}^{-1}$ , V = 50 mL, and initial pH = 5.6.

In order to establish the participation of radical species in the heterogeneous catalysis, experiments in the presence of MeOH or TBA were performed (Figure 5b). A strong inhibition of CIP degradation was found in the presence of methanol, while tert-butanol slightly decreased the pollutant removal. These results indicate a high participation of sulfate radicals and a low participation of hydroxyl radicals in the CIP elimination by the MMO/PMS system [18]. The generation of sulfate radicals (the main product responsible for CIP degradation) can be rationalized considering that the interaction of PMS with cobalt and copper ions on the MMO surface leads to sulfate radicals. Initially,  $=\text{Co}^{2+}$  and  $\text{Cu}^+$  can transfer an electron to PMS, forming  $\text{SO}_4^{\bullet-}$  (Equations (4) and (5)). The presence of  $\text{Cu}^+$  in the catalyst can also contribute to the inner reduction in  $=\text{Co}^{3+}$  because of the lower redox potential of  $=\text{Cu}^{2+}/=\text{Cu}^+$  ( $E^\circ = 0.16 \text{ V}$ ) than that of  $=\text{Co}^{3+}/\text{Co}^{2+}$  ( $E^\circ = 1.81 \text{ V}$ ) (Equation (6)) [22]; whereas,  $\text{Cr}_2\text{O}_4^{2-}$  acts as the carrier/support for the active metal for PMS decomposition. Furthermore, hydroxyl radicals can be formed through the interaction of sulfate radicals with water or hydroxyl anion in the liquid medium (Equations (7) and (8)) [24]. However, as also indicated by the results in Figure 5b, a small participation of  $\text{HO}\bullet$  occurred.



XRD, BET, and XPS analyses for the MMO after use in the activation of PMS were also performed (Figures S3–S5 and Table S2). These analyses showed that, under the experimental conditions, the structure, area, and composition of the surface of the used MMO were very similar to those of the MMO before use, indicating that this material effectively acted as a catalyst for PMS activation.

### 2.5. Primary Transformations of CIP Using the MMO/PMS System

In addition to the characterization of the used MMO, the action of radicals on the CIP structure was elucidated by determining the primary transformations by using LC–MS analyses (Figure 6). Three by-products of the CIP transformation were identified (P1, P2, and P3, for which MS spectra are presented in Figures S6–S9). The attacks of sulfate (or hydroxyl) radicals on the CIP structure led to the opening (P1) and the oxidation of the piperazyl ring (P2). Moreover, hydroxylations on the quinolone moiety induced the formation of P3. These transformation products are consistent with the computational calculations that have been reported in the literature [28], which indicate that piperazyl and the benzene rings are electron-rich moieties that are very susceptible to the reaction with radicals.

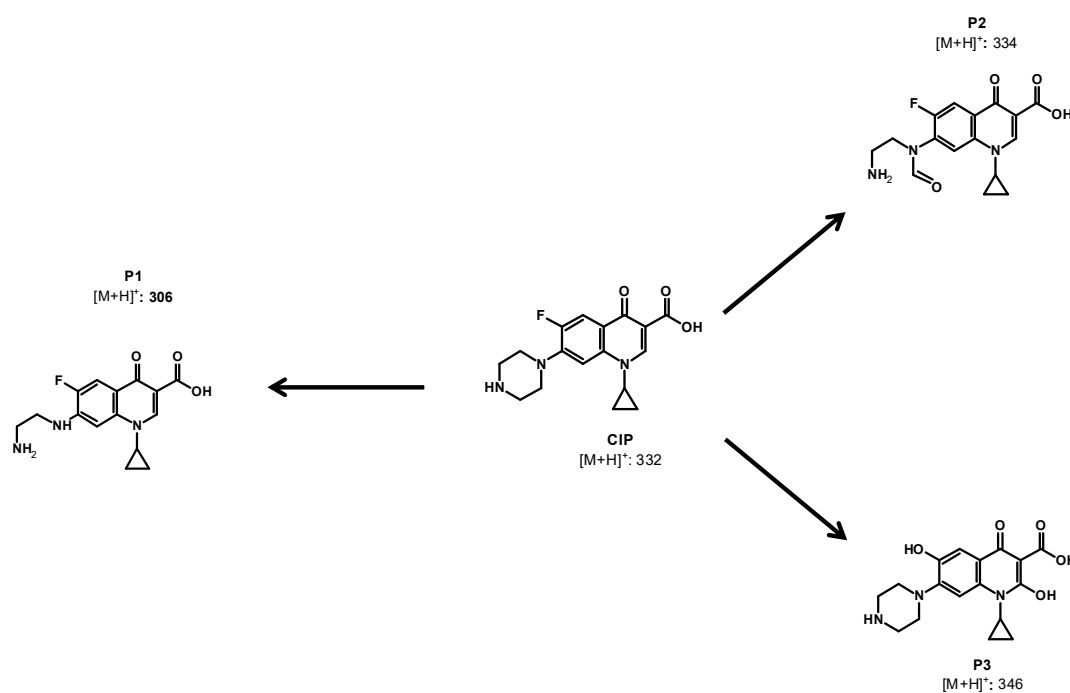


**Figure 6.** Primary transformation products from CIP degradation. Experimental conditions: CIP = 30.6  $\mu\text{mol L}^{-1}$ , MMO = 0.2  $\text{g L}^{-1}$ , PMS = 500  $\mu\text{mol L}^{-1}$ , V = 50 mL, and initial pH = 5.6.

The formation of P1 and P2 can start with an electron transfer from the electron-rich piperazyl ring to the sulfate radicals [24,29–31]. The initial attack of  $\text{SO}_4^{\bullet-}$  at the secondary amine on the piperazyl moiety produces a cation radical, then, it experiences an  $\alpha$ -deprotonation [32], with the posterior water reaction producing an intermediate alcohol. Such alcohol leads to imine and aldehyde groups. Subsequently, the hydrolysis of imine yields P2. In addition, the cation radical, which is initially generated from a radical attack to tertiary amine on the piperazyl ring, reacts with water, forming a secondary hydroxylamine. This hydroxylamine can evolve into a di-imine intermediate; moreover, afterward, the water can promote di-imine hydrolysis, yielding P1 [28,33]. Furthermore, the sulfate radical can also attack C–C  $\pi$ -systems [25]. As the quinolone system is an electron-rich region of CIP, an electron abstraction from such a moiety, followed by a reaction with water, generates the hydroxylation product (P3) [28,34].

The primary transformations induced by the MMO/PMS system could modify the antimicrobial activity (AA) associated with CIP. Therefore, in order to establish the possibility of the AA decreasing, theoretical analyses were carried out. Table 3 compares the probability (Pa) of the parent antibiotic and its primary products of being active. Biological activities such as the anti-infective, antibiotic quinolone-like DNA synthesis inhibitor, DNA gyrase inhibitor, DNA topoisomerase IV inhibitor, and topoisomerase II inhibitor (which are recognized as the main antimicrobial action mechanisms [35]) were considered.

It can be noted that all of the Pa values corresponding to the considered activities for the three primary products were lower than those for the CIP, suggesting a decrease in the AA after the treatment with the MMO/PMS system. This is also supported by the structural changes introduced to the parent antibiotic. The treatment modified the piperazyl ring and the quinolone group of CIP (Figure 6) that control the antibacterial potency, the action spectrum, and the efflux inhibition [36]. The cleavage of the piperazyl (P1) or oxidation (P2) may alter the acid/base speciation, decrease the lipophilicity, and diminish the cell permeability [37] and the linkage to bacterial DNA topoisomerases or DNA gyrase [38]. Moreover, the hydroxylation of the quinolone core (P3) and the loss of fluorine could also diminish the potency and the binding properties of the antibiotic [36].

**Table 3.** Predictions of the biological activity for CIP and its primary transformation products.

Biological Activity <sup>+</sup>	Pa * for CIP	Pa for P1	Pa for P2	Pa for P3
Anti-infective	0.823	0.448	0.275	0.360
DNA synthesis inhibitor	0.786	0.529	0.493	0.500
Topoisomerase II inhibitor	0.751	0.581	0.505	0.313
Antibiotic Quinolone-like	0.567	0.172	0.138	0.053
DNA gyrase inhibitor	0.468	0.166	0.067	0.122
DNA topoisomerase IV inhibitor	0.222	0.070	0.052	0.031

<sup>+</sup> The predictions of biological activity were carried out on the PASS software (free online version, [www.pharmaexpert.ru/passonline/index.php](http://www.pharmaexpert.ru/passonline/index.php), accessed on 28 April 2023) [39]. \* Pa: probability to be active.

## 2.6. Reuse of the Catalyst and Treatment in a Complex Matrix CIP Degradation and Using the MMO/PMS System

The reusability of the catalyst and its performance in a matrix that is more complex than distilled water are influential factors for assessing the extent of the degrading processes [22,40]. Thus, the reuse test of the MMO catalyst in CIP degradation was considered. In addition, the treatment of CIP in synthetic hospital wastewater (HWW), using the MMO/PMS system was performed. Figure 7a presents the degradation of CIP after three reuse cycles of the catalyst. The CIP degradation rate decreased slightly after each cycle.

As occurs with other catalysts employed for PMS activation, the catalyst could adsorb some molecules of CIP, or its byproducts, onto the surface during the degradation process [41,42], and such adsorbed substances are not completely removed in the recycling tests. Therefore, a small portion of the active sites is occupied, resulting in a slight decrease in the catalytic performance of the MMO to activate the PMS and produce the radicals that are responsible for CIP degradation (see the  $S_{BET}$  results for the used MMO in Table 2, which had a slightly lower  $S_{BET}$  than the  $\Phi y$  material). However, it can be highlighted that this slight fall did not affect the application of the material significantly, because the MMO/PMS system was able to achieve up to 90% of pollutant removal, even after the third reuse cycle.

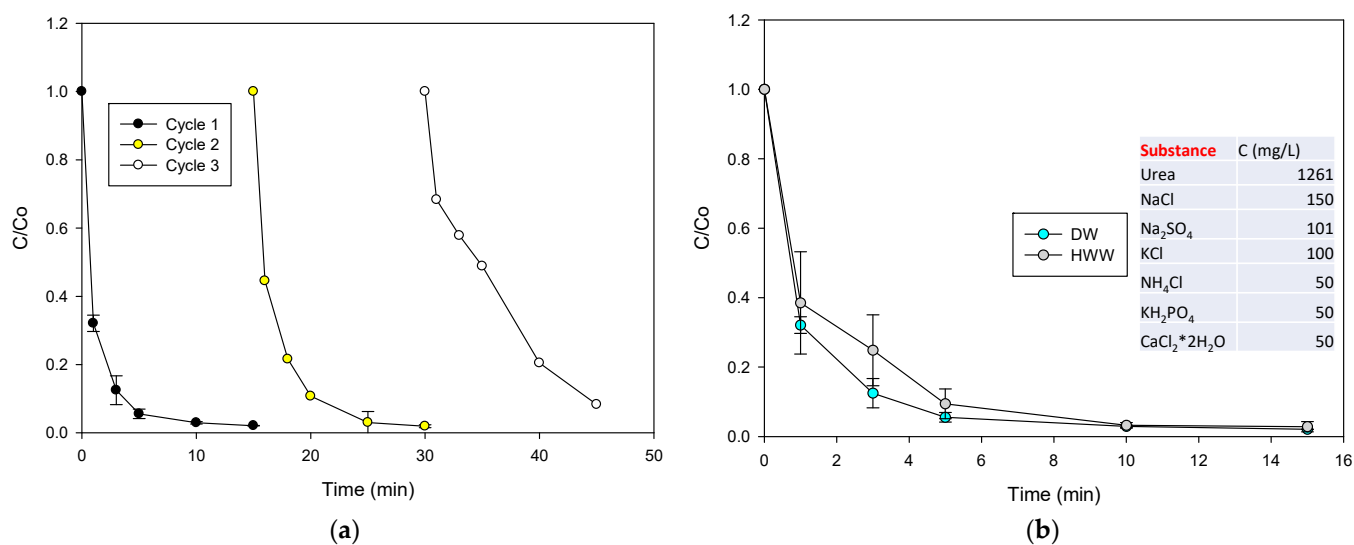
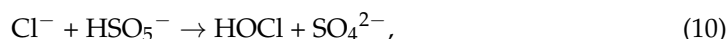


**Figure 7.** The extent of the treatment of CIP with the MMO/PMS system. (a) Reusability of the catalyst in the CIP degradation with the MMO/PMS system and (b) the degradation of CIP in HWW using the MMO/PMS system. Experimental conditions: CIP = 30.6  $\mu\text{mol L}^{-1}$ , MMO = 0.2 g  $\text{L}^{-1}$ , PMS = 500  $\mu\text{mol L}^{-1}$ , V = 50 mL, and initial pH = 5.6.

Regarding the treatment of CIP in the HWW (Figure 7b), it can be noted that the pollutant degradation was close to that obtained in the distilled water (DW). This could be explained by the fact that the MMO/PMS system can produce a lot of radicals to degrade the target molecule, with a low competence of the other matrix components. Moreover, the reaction of sulfate radicals with chloride anions is possible, which leads to the formation of chlorine radicals (Equation (9), [43]) that degrade CIP, even producing intermediates such as P1 (Figure 6) [44]. Additionally, PMS can also react with  $\text{Cl}^-$  to produce HOCl (Equation (10)) [45–47]. Hypochlorous acid is a well-known oxidizing agent capable of promoting CIP degradation [48,49]. Indeed, the interaction of CIP with HOCl also leads to the opening of the piperazyl ring (P1 in Figure 6) as the major transformation product [48].



### 3. Materials and Methods

#### 3.1. Reagents

Oxone<sup>®</sup> ( $\text{KHSO}_5$ ,  $0.5\text{KHSO}_4$ , and  $0.5\text{K}_2\text{SO}_4$ ) was purchased from Sigma. The ciprofloxacin hydrochloride (CIP) was provided by Laproff Laboratories. The acetonitrile, sodium azide, sodium bicarbonate, sodium chloride, sodium dihydrogen phosphate, sodium hydroxide, sodium sulfate, sulfuric acid, methyl orange, and urea were provided by Merck. The ammonium chloride, calcium chloride dihydrate, magnesium chloride hexahydrate, and sodium citrate dihydrate were obtained from PanReac. The formic acid was obtained from Carlo Erba.

It is important to mention that CIP was selected as a representative pollutant because it is an antibiotic that is consumed worldwide, frequently found in diverse wastewater and environmental water [50]. CIP has particular concerns surrounding it due to its adverse effects on ecosystems. For example, CIP can promote the development and proliferation of antibiotic-resistant bacteria [51]. Additionally, this antibiotic belongs to the European watch list of substances for union-wide monitoring in water policy (Decision 2020/1161) [52].

The synthesis of the  $\Phi\gamma$  material consisted of generating a laminar phase through the hydrothermal method, mixing the precursors of the metals required in the following

specific molar ratio:  $\text{CrO}_3:0.5\text{Cu}(\text{NO}_3)_2 \cdot 3\text{H}_2\text{O}:0.5\text{Co}(\text{NO}_3)_2 \cdot 6\text{H}_2\text{O}:\text{NH}_4\text{OH}:164\text{H}_2\text{O}$ . The solutions of  $\text{CrO}_3$  (Merck, Darmstadt, Germany, 99.0%),  $\text{Cu}(\text{NO}_3)_2 \cdot 3\text{H}_2\text{O}$  (Merck, 99.0%), and  $\text{Co}(\text{NO}_3)_2 \cdot 6\text{H}_2\text{O}$  (J.T Baker, 99.3%) were prepared in Teflon beakers. The pink cobalt solution was added in by stirring it into the blue copper solution, and, in the same way, the resulting mixture was added to the brown chromium solution. Afterward, the  $\text{NH}_4\text{OH}$  (JT Baker, 28%) solution was added drop by drop, obtaining a brown gel that was stirred for 45 min and packed to a stainless-steel autoclave with a liner of Teflon. The reaction was carried out in an oven at  $100\text{ }^\circ\text{C}$  for 3 days. The obtained solid was filtered, washed to neutral pH, and dried at  $60\text{ }^\circ\text{C}$ . To obtain the mixed metal oxides of copper, cobalt, and chromium (i.e., MMO), the laminar phase (i.e.,  $\Phi\text{y}$ ) was calcinated at  $450\text{ }^\circ\text{C}$  for 1 h in an oven (Fisher Scientific, Pittsburgh, PA, USA) using an increase of  $10\text{ }^\circ\text{C}/\text{min}$  up to reach the calcination temperature.

### 3.2. Reaction Systems for Pollutant Removal

The catalytic tests were performed using a beaker in a magnetic stirring system (Figure S10, in the Supplementary Materials). A pollutant solution (50 mL) was considered, and the solid material ( $\Phi\text{y}$  or MMO) and PMS were added at  $0.2\text{ g L}^{-1}$  and  $500\text{ }\mu\text{mol L}^{-1}$ , respectively. The concentrations of catalysts and peroxides were chosen based on previous works, which report the use of oxidants (e.g., PMS) in the range of  $50\text{--}1000\text{ }\mu\text{mol L}^{-1}$  and  $0.25\text{--}1.0\text{ g L}^{-1}$  for the solid catalysts as the suitable amounts for the activation process development [53–58].

### 3.3. Analyses

The X-ray diffraction analysis (XRD) was carried out in an XPert PANanalytical Empyrean series ii (Ni-filtered  $\text{Cu K}\alpha$  radiation), with a time-per-step of 50 s and a step size of  $0.05^\circ$  between  $5$  and  $80^\circ 2\theta$ . The composition of the solid samples was analyzed in a Thermo Scientific Ice 3000 atomic absorption (AA) spectrometer. A total of 20 mg of sample was weighed and subject to acid digestion with 2.5  $\mu\text{L}$  of concentrated HF at room temperature. The solutions were graduated to 100 mL and dilutions were made for the different metals. The thermograms were collected using a TA Instruments Discovery 650 analyzer and 25 mg of sample was weighed and heating to  $800\text{ }^\circ\text{C}$ , with a ramp of  $10\text{ }^\circ\text{C min}^{-1}$  and airflow of  $40\text{ mL min}^{-1}$ . An ASAP2020plus sortometer was used to obtain the nitrogen adsorption–desorption isotherms (NADI) after degassing 200 mg of sample at  $250\text{ }^\circ\text{C}$  for 4 h at  $10\text{ }\mu\text{m Hg}$ . The specific surface area BET ( $S_{\text{BET}}$ ) was calculated by applying the Rouquerol method and a t plot was used for the external surface ( $S_{\text{ext}}$ ) area and micropore volume ( $V_{\text{micro}}$ ). The total pore volume ( $V_{\text{total}}$ ) was determined at  $0.99\text{ p}/\text{p}_0$ . The morphology of the materials was determined through scanning electron microscopy (SEM) using a JEOL JSM-6490LV (at 20 kV and  $10,000\times$  magnification).

The surface chemical information was determined by X-ray photoelectron spectroscopy (XPS) using a PHOIBOS 150 1D-DLD analyzer and monochromatic  $\text{Al-K}\alpha$  radiation (1487 eV) operated at 10 W. The XPS spectra were recorded with a pass energy of 83.36 eV and step size of 1 eV for general spectrums and a pass energy of 20 eV and step size of 0.1 eV for high-resolution spectra. The charge compensation was achieved by a low-energy electron flood gun (3 eV cathode voltage and 20 mA emission current). Adventitious C1s core level line was selected as the reference to calibrate the energy scale. The spectra were analyzed by using a Gaussian–Lorentzian blend (GL 20–30%) and a Shirley-type background subtraction.

The CIP evolution was followed using liquid chromatography. A Thermo Scientific Ultimate 3000 UHPLC, equipped with a DAD detector and an Acclaim<sup>TM</sup> 120 Thermo Scientific column (C18, 5  $\mu\text{m}$ ,  $4.6 \times 150\text{ mm}$ ), was utilized. In all cases, 20  $\mu\text{L}$  was the injection volume. As the mobile phase, a 15/85 mixture of acetonitrile/formic acid ( $10\text{ mmol L}^{-1}$ ) at  $1.0\text{ mL min}^{-1}$  was used. The detection wavelength was 278 nm. The primary transformation products from the CIP degradation were established using an HPLC Agilent 1200 series, coupled with an Agilent LC/MSD VL SQ mass spectrometer. The column and

mobile phase operated at the conditions utilized for monitoring the pharmaceutical evolution. The injection volume was 10  $\mu\text{L}$ , and the mass spectrometer detector was operated in positive ion mode [59]. In the case of MO, this was followed by measuring the absorbance at 465 nm using a UV5 Mettler-Toledo spectrophotometer.

For the target pollutant and its primary transformation products, predictions of their antimicrobial biological activity were carried out with PASS software (free online version) [39], which is based on analyses of structure–activity relationships [39]. The chemical structures of these substances were uploaded to the PASS software in the SMILE format individually (Table S3). Then, the PASS software output the values of the probability of biological activities (Pa) for the tested substances.

#### 4. Conclusions

The chromate of copper and cobalt material ( $\Phi\text{y}$ ) was effectively synthesized by the hydrothermal method. The  $\Phi\text{y}$  phase had a high crystalline nature, as shown by XRD and the laminar characteristics evidenced by its specific surface area. Additionally, the total pore volume demonstrated the small particle size, due to the space between the layers. This material showed a good ability to promote the degradation of CIP; however, the interaction with PMS destabilized this solid material, leaching metals and calling into question the practical application of  $\Phi\text{y}$ . Interestingly, the calcination of  $\Phi\text{y}$  produced an MMO, which had textural characteristics inherited from the laminar phase. Despite the elimination of microporosity, the MMO retained the interparticle mesoporosity. In addition, the phase of  $\text{Co}_x\text{Cu}_{1-x}\text{Cr}_2\text{O}_4$  formed by calcination was favorably located on the surface of the material. Additionally, the MMO showed a degradation efficiency similar to that reported for cobalt-doped metal oxide/hydroxide substrates for heterogeneous PMS activation, with the advantage of no leaching of cobalt, which is a typical concern for the other substrates.

The MMO also presented a high activating capability toward PMS, stability, and no leaching of metals. In the MMO/PMS system, the generated sulfate radical species was responsible for the CIP degradation, as evidenced by the tests with scavengers (methanol and tert-butanol). The produced sulfate radical reacted with the target pollutant, opening the piperazyl ring of CIP and hydroxylating the quinolone moiety as the primary transformations (which decreased the biological activity according to the theoretical analyses). The MMO exhibited good reusability for the activation of PMS to degrade CIP, even after the third run. Furthermore, the MMO/PMS process showed a high degrading capability toward CIP in HWW, indicating that the complex matrix induced low competing effects. It can be remarked that this research has provided valuable information on the instability of Co- and Cu-based materials under interaction with PMS and a strategy to overcome the leaching limitation and obtain a proper catalyst (from  $\Phi\text{y}$  calcination) for promoting CIP transformation into more environmentally friendly compounds.

**Supplementary Materials:** The following supporting information can be downloaded at: <https://www.mdpi.com/article/10.3390/molecules28114536/s1>, Figure S1: XRD Rietveld refinement for MMO; Figure S2:  $\text{N}_2$ -adsorption isotherm and SEM for MMO; Figure S3: XRD analyses for the used MMO; Figure S4:  $\text{N}_2$ -adsorption isotherm for the used MMO; Figure S5: XPS for the used MMO; Figures S6–S9: MS spectra; Figure S10: Reaction system; Table S1: Cobalt leaching from  $\Phi\text{y}$ ; Table S2: Comparison of textural properties of the MMO before and after use; and Table S3: CIP and its degradation products in SMILES format.

**Author Contributions:** Conceptualization, E.A.S.-G., D.A.H.-A., R.A.T.-P. and A.E.-I.; methodology, E.A.S.-G. and C.M.-M.; formal analysis, E.A.S.-G. and C.M.-M.; investigation, E.A.S.-G. and C.M.-M.; resources, D.A.H.-A., R.A.T.-P. and A.E.-I.; data curation, E.A.S.-G. and C.M.-M.; writing—original draft preparation, E.A.S.-G.; writing—review and editing, D.A.H.-A., R.A.T.-P. and A.E.-I.; supervision, D.A.H.-A., R.A.T.-P. and A.E.-I.; project administration, D.A.H.-A.; funding acquisition, D.A.H.-A., R.A.T.-P. and A.E.-I. All authors have read and agreed to the published version of the manuscript.

**Funding:** This research was funded by COMITÉ PARA EL DESARROLLO DE LA INVESTIGACIÓN-CODI-UNIVERSIDAD DE ANTIOQUIA UDEA, grant number “Catalizadores de Óxidos Mixtos Funcionalizados sobre Nanotubos de Carbón y su Evaluación en la Reacción de Oxidación de Tolueno, 2020-32251”, and MINCIENCIAS COLOMBIA, grant number “Program to improve the quality of irrigation water through the elimination of emerging contaminants by advanced oxidation processes (PRO-CEC-AGUA), 1115-852-69594.” The APC was funded by Universidad de Antioquia UdeA.

**Institutional Review Board Statement:** Not applicable.

**Informed Consent Statement:** Not applicable.

**Data Availability Statement:** Data will be available by request via email to the corresponding authors.

**Acknowledgments:** The authors thank Valentina Vásquez-Sánchez for her help in the preparation of some experimental tests.

**Conflicts of Interest:** The authors declare no conflict of interest.

**Sample Availability:** Samples of the compounds are not available from the authors.

## References

1. Brausch, J.M.; Connors, K.; Brooks, B.W.; Rand, G.M. Human pharmaceuticals in the aquatic environment: A review of recent toxicological studies and considerations for toxicity testing. *Rev. Environ. Contam. Toxicol.* **2012**, *218*, 1–99. [CrossRef]
2. Khetan, S.K.; Collins, T.J. Human pharmaceuticals in the aquatic environment: A challenge to green chemistry. *Chem. Rev.* **2007**, *107*, 2319–2364. [CrossRef]
3. Rizzo, L.; Manaia, C.; Merlin, C.; Schwartz, T.; Dagot, C.; Ploy, M.C.; Michael, I.; Fatta-Kassinos, D. Urban wastewater treatment plants as hotspots for antibiotic resistant bacteria and genes spread into the environment: A review. *Sci. Total Environ.* **2013**, *447*, 345–360. [CrossRef] [PubMed]
4. Botero-Coy, A.M.; Martínez-Pachón, D.; Boix, C.; Rincón, J.R.; Castillo, N.; Arias-Marín, L.P.; Manrique-Losada, L.; Torres-Palma, R.A.; Moncayo-Lasso, A.; Hernández, F. An investigation into the occurrence and removal of pharmaceuticals in colombian wastewater. *Sci. Total Environ.* **2018**, *62*, 842–853. [CrossRef] [PubMed]
5. Hernández, F.; Ibáñez, M.; Botero-Coy, A.-M.; Bade, R.; Bustos-López, M.C.; Rincón, J.; Moncayo, A.; Bijlsma, L. LC-QTOF MS screening of more than 1,000 licit and illicit drugs and their metabolites in wastewater and surface waters from the area of Bogotá, Colombia. *Anal. Bioanal. Chem.* **2015**, *407*, 6405–6416. [CrossRef]
6. Saravanan, A.; Deivayanai, V.C.; Kumar, P.S.; Rangasamy, G.; Hemavathy, R.V.; Harshana, T.; Gayathri, N.; Alagumalai, K. A detailed review on advanced oxidation process in treatment of wastewater: Mechanism, challenges and future outlook. *Chemosphere* **2022**, *308*, 136524. [CrossRef] [PubMed]
7. Lee, J.; Von Gunten, U.; Kim, J.H. Persulfate-Based Advanced Oxidation: Critical Assessment of Opportunities and Roadblocks. *Environ. Sci. Technol.* **2020**, *54*, 3064–3081. [CrossRef]
8. Waclawek, S.; Lutze, H.V.; Grübel, K.; Padil, V.V.T.; Černík, M.; Dionysiou, D.D. Chemistry of persulfates in water and wastewater treatment: A review. *Chem. Eng. J.* **2017**, *330*, 44–62. [CrossRef]
9. Li, B.; Wang, Y.F.; Zhang, L.; Xu, H.Y. Enhancement strategies for efficient activation of persulfate by heterogeneous cobalt-containing catalysts: A review. *Chemosphere* **2022**, *291*, 132954. [CrossRef]
10. Zheng, X.; Niu, X.; Zhang, D.; Lv, M.; Ye, X.; Ma, J.; Lin, Z.; Fu, M. Metal-based catalysts for persulfate and peroxymonosulfate activation in heterogeneous ways: A review. *Chem. Eng. J.* **2022**, *429*, 132323. [CrossRef]
11. Bokare, A.D.; Choi, W. Chromate-induced activation of hydrogen peroxide for oxidative degradation of aqueous organic pollutants. *Environ. Sci. Technol.* **2010**, *44*, 7232–7237. [CrossRef] [PubMed]
12. Liu, L.; Li, Y.; Li, W.; Lan, Y.; Li, Y. CrPO<sub>4</sub> as a recycled material supported Co<sub>3</sub>O<sub>4</sub> as an efficient peroxymonosulfate catalyst for phenacetin elimination from aqueous solution. *Chem. Eng. J.* **2022**, *433*, 133558. [CrossRef]
13. Zhong, Y.; Chen, Z.-F.; Yan, S.-C.; Wei, W.-W.; Zhang, Q.; Liu, G.; Cai, Z.; Yu, L. Photocatalytic transformation of climbazole and 4-chlorophenol formation using a floral array of chromium-substituted magnetite nanoparticles activated with peroxymonosulfate. *Environ. Sci. Nano* **2019**, *6*, 2986–2999. [CrossRef]
14. Arboleda, J.; Echavarría, A.; Palacio, L.A. Synthesis and characterization of (NH<sub>4</sub>)<sub>1.5</sub>Cu<sub>2</sub>Cr<sub>2</sub>O<sub>8</sub>(OH)<sub>1.5</sub>·H<sub>2</sub>O. *Powder Diffr.* **2009**, *24*, 244–246. [CrossRef]
15. Kiejza, D.; Kotowska, U.; Poli, W.; Karpi, J. Peracids-New oxidants in advanced oxidation processes: The use of peracetic acid, peroxymonosulfate, and persulfate salts in the removal of organic micropollutants of emerging concern—A review. *Sci. Total Environ.* **2021**, *790*, 148195. [CrossRef]
16. National Library of Medicine Methyl Orange Properties. Available online: <https://pubchem.ncbi.nlm.nih.gov/compound/23673835> (accessed on 23 February 2023).
17. Rao, V.P.R.; Satyanarayana, D.; Suryanarayana, A. Methyl orange as a redox indicator in titrations with ceric ammonium nitrate in perchloric acid. *Fresenius' Z. Anal. Chem.* **1962**, *191*, 202–204. [CrossRef]

18. He, X.; Mezyk, S.P.; Michael, I.; Fatta-Kassinos, D.; Dionysiou, D.D. Degradation kinetics and mechanism of  $\beta$ -lactam antibiotics by the activation of  $\text{H}_2\text{O}_2$  and  $\text{Na}_2\text{S}_2\text{O}_8$  under UV-254nm irradiation. *J. Hazard. Mater.* **2014**, *279*, 375–383. [CrossRef]
19. Anipsitakis, G.P.; Dionysiou, D.D. Degradation of organic contaminants in water with sulfate radicals generated by the conjunction of peroxymonosulfate with cobalt. *Environ. Sci. Technol.* **2003**, *37*, 4790–4797. [CrossRef]
20. Yu, D.; He, J.; Xie, T.; Xu, Q.; Li, G.; Du, L.; Huang, J.; Yang, J.; Li, W.; Wang, J. Peroxymonosulfate activation using a composite of copper and nickel oxide coated on SBA-15 for the removal of sulfonamide antibiotics. *Environ. Res.* **2022**, *206*, 112301. [CrossRef]
21. Ball, D.L.; Edwards, J.O. The catalysis of the decomposition of Caro's acid. *J. Phys. Chem.* **1958**, *62*, 343–345. [CrossRef]
22. Gao, Q.; Wang, G.; Chen, Y.; Han, B.; Xia, K.; Zhou, C. Utilizing cobalt-doped materials as heterogeneous catalysts to activate peroxymonosulfate for organic pollutant degradation: A critical review. *Environ. Sci. Water Res. Technol.* **2021**, *7*, 1197–1211. [CrossRef]
23. Xie, R.C.; Batchelor-McAuley, C.; Rauwel, E.; Rauwel, P.; Compton, R.G. Electrochemical Characterisation of Co@Co(OH)<sub>2</sub> Core-Shell Nanoparticles and their Aggregation in Solution. *ChemElectroChem* **2020**, *7*, 4259–4268. [CrossRef]
24. Matzek, L.W.; Carter, K.E. Activated persulfate for organic chemical degradation: A review. *Chemosphere* **2016**, *151*, 178–188. [CrossRef]
25. Anipsitakis, G.P.; Dionysiou, D.D.; Gonzalez, M.A. Cobalt-mediated activation of peroxymonosulfate and sulfate radical attack on phenolic compounds. Implications of chloride ions. *Environ. Sci. Technol.* **2006**, *40*, 1000–1007. [CrossRef] [PubMed]
26. Rietveld, H.M. A profile refinement method for nuclear and magnetic structures. *J. Appl. Crystallogr.* **1969**, *2*, 65–71. [CrossRef]
27. Awala, H.; Gilson, J.-P.; Retoux, R.; Boullay, P.; Goupil, J.-M.; Valtchev, V.; Mintova, S. Template-free nanosized faujasite-type zeolites. *Nat. Mater.* **2015**, *14*, 447–451. [CrossRef] [PubMed]
28. Serna-Galvis, E.A.; Ferraro, F.; Silva-Agredo, J.; Torres-Palma, R.A. Degradation of highly consumed fluoroquinolones, penicillins and cephalosporins in distilled water and simulated hospital wastewater by UV254 and UV254/persulfate processes. *Water Res.* **2017**, *122*, 128–138. [CrossRef]
29. Liang, C.; Su, H.W. Identification of sulfate and hydroxyl radicals in thermally activated persulfate. *Ind. Eng. Chem. Res.* **2009**, *48*, 5558–5562. [CrossRef]
30. Clennan, E.L.; Pace, A. Advances in singlet oxygen chemistry. *Tetrahedron* **2005**, *61*, 6665–6691. [CrossRef]
31. Salma, A.; Thorøe-Boveleth, S.; Schmidt, T.C.; Tuerk, J. Dependence of transformation product formation on pH during photolytic and photocatalytic degradation of ciprofloxacin. *J. Hazard. Mater.* **2016**, *313*, 49–59. [CrossRef]
32. Hu, J.; Wang, J.; Nguyen, T.H.; Zheng, N. The chemistry of amine radical cations produced by visible light photoredox catalysis. *Beilstein J. Org. Chem.* **2013**, *9*, 1977–2001. [CrossRef]
33. Dennis, W.; Hull, L.; Rosenblatt, D. Oxidations of amines. IV. Oxidative fragmentation. *J. Org. Chem.* **1967**, *32*, 3783–3787. [CrossRef]
34. Nicolaescu, A.R.; Wiest, O.; Kamat, P.V. Radical-induced oxidative transformation of quinoline. *J. Phys. Chem. A* **2003**, *107*, 427–433. [CrossRef]
35. DrugBank Ciprofloxacin. Available online: <https://go.drugbank.com/drugs/DB00537> (accessed on 19 January 2023).
36. Andersson, M.I.; MacGowan, A.P. Development of the quinolones. *J. Antimicrob. Chemother.* **2003**, *51* (Suppl. S1), 1–11. [CrossRef]
37. Paul, T.; Dodd, M.C.; Strathmann, T.J. Photolytic and photocatalytic decomposition of aqueous ciprofloxacin: Transformation products and residual antibacterial activity. *Water Res.* **2010**, *44*, 3121–3132. [CrossRef]
38. Alvero, F.L.; Pan, X.; Morris, J.E.; Manzo, R.H.; Fisher, L.M. Engineering the Specificity of Antibacterial Fluoroquinolones: Benzenesulfonamide Modifications at C-7 of Ciprofloxacin Change Its Primary Target in Streptococcus pneumoniae from Topoisomerase IV to Gyrase. *Antimicrob. Agents Chemother.* **2000**, *44*, 320–325. [CrossRef] [PubMed]
39. W2D Team-PharmaExpert PASS Online. Available online: <http://www.pharmaexpert.ru/passonline/index.php> (accessed on 2 May 2021).
40. Serna-Galvis, E.A.; Martínez-Mena, Y.L.; Arboleda-Echavarría, J.; Hoyos-Ayala, D.A.; Echavarría-Isaza, A.; Torres-Palma, R.A. Zeolite 4A activates peroxymonosulfate toward the production of singlet oxygen for the selective degradation of organic pollutants. *Chem. Eng. Res. Des.* **2023**, *193*, 121–131. [CrossRef]
41. Sun, Q.; Wang, X.; Liu, Y.; Xia, S.; Zhao, J. Activation of peroxymonosulfate by a floating oxygen vacancies-CuFe<sub>2</sub>O<sub>4</sub> photocatalyst under visible light for efficient degradation of sulfamethazine. *Sci. Total Environ.* **2022**, *824*, 153630. [CrossRef]
42. Liu, L.; Li, Y.; Pang, Y.; Lan, Y.; Zhou, L. Activation of peroxymonosulfate with CuCo<sub>2</sub>O<sub>4</sub>@kaolin for the efficient degradation of phenacetin. *Chem. Eng. J.* **2020**, *401*, 126014. [CrossRef]
43. Liu, Y.; He, X.; Fu, Y.; Dionysiou, D.D. Kinetics and mechanism investigation on the destruction of oxytetracycline by UV-254 nm activation of persulfate. *J. Hazard. Mater.* **2016**, *305*, 229–239. [CrossRef] [PubMed]
44. Deng, J.; Wu, G.; Yuan, S.; Zhan, X.; Wang, W.; Hu, Z.H. Ciprofloxacin degradation in UV/chlorine advanced oxidation process: Influencing factors, mechanisms and degradation pathways. *J. Photochem. Photobiol. A Chem.* **2019**, *371*, 151–158. [CrossRef]
45. Zhou, Y.; Jiang, J.; Gao, Y.; Pang, S.Y.; Ma, J.; Duan, J.; Guo, Q.; Li, J.; Yang, Y. Oxidation of steroid estrogens by peroxymonosulfate (PMS) and effect of bromide and chloride ions: Kinetics, products, and modeling. *Water Res.* **2018**, *138*, 56–66. [CrossRef] [PubMed]
46. Lou, X.Y.; Guo, Y.G.; Xiao, D.X.; Wang, Z.H.; Lu, S.Y.; Liu, J.S. Rapid dye degradation with reactive oxidants generated by chloride-induced peroxymonosulfate activation. *Environ. Sci. Pollut. Res.* **2013**, *20*, 6317–6323. [CrossRef]

47. Liu, T.; Zhang, D.; Yin, K.; Yang, C.; Luo, S.; Crittenden, J.C. Degradation of thiacloprid via unactivated peroxymonosulfate: The overlooked singlet oxygen oxidation. *Chem. Eng. J.* **2020**, *388*, 124264. [[CrossRef](#)]
48. Dodd, M.C.; Shah, A.D.; Von Gunten, U.; Huang, C.H. Interactions of fluoroquinolone antibacterial agents with aqueous chlorine: Reaction kinetics, mechanisms, and transformation pathways. *Environ. Sci. Technol.* **2005**, *39*, 7065–7076. [[CrossRef](#)]
49. Serna-Galvis, E.A.; Jojoa-Sierra, S.D.; Berrio-Perlaza, K.E.; Ferraro, F.; Torres-Palma, R.A. Structure-reactivity relationship in the degradation of three representative fluoroquinolone antibiotics in water by electrogenerated active chlorine. *Chem. Eng. J.* **2017**, *315*, 552–561. [[CrossRef](#)]
50. Patel, M.; Kumar, R.; Kishor, K.; Mlsna, T.; Pittman, C.U.; Mohan, D. Pharmaceuticals of emerging concern in aquatic systems: Chemistry, occurrence, effects, and removal methods. *Chem. Rev.* **2019**, *119*, 3510–3673. [[CrossRef](#)]
51. Sidhu, H.; Bae, H.; Ogram, A.; Connor, G.O. Azithromycin and Ciprofloxacin Can Promote Antibiotic. *Appl. Environ. Microbiol.* **2021**, *87*, e00373-21. [[CrossRef](#)]
52. European Union, Decision 2020/1161/EU Commission Implementing Decision (EU) 2020/1161-4 August 2020-establishing a watch list of substances for Union-wide monitoring in the field of water policy pursuant to Directive 2008/105/EC of the European Parliament and of the Council. *Off. J. Eur. Union* **2020**, *257*, 32–35.
53. Dai, Y.; Peng, Q.; Liu, K.; Tang, X.; Zhou, M.; Jiang, K.; Zhu, B. Activation of peroxymonosulfate by chrysotile to degrade dyes in water: Performance enhancement and activation mechanism. *Minerals* **2021**, *11*, 400. [[CrossRef](#)]
54. Li, C.; Huang, Y.; Dong, X.; Sun, Z.; Duan, X.; Ren, B.; Zheng, S.; Dionysiou, D.D. Highly efficient activation of peroxymonosulfate by natural negatively-charged kaolinite with abundant hydroxyl groups for the degradation of atrazine. *Appl. Catal. B Environ.* **2019**, *247*, 10–23. [[CrossRef](#)]
55. Fu, X.; Zhang, J.; Zhao, H.; Zhang, S.; Nie, T.; Zhang, Y.; Lu, J. Enhanced peroxymonosulfate activation by coupling zeolite-supported nano-zero-valent iron with weak magnetic field. *Sep. Purif. Technol.* **2020**, *230*, 115886. [[CrossRef](#)]
56. Sun, X.; Xu, D.; Dai, P.; Liu, X.; Tan, F.; Guo, Q. Efficient degradation of methyl orange in water via both radical and non-radical pathways using Fe-Co bimetal-doped MCM-41 as peroxymonosulfate activator. *Chem. Eng. J.* **2020**, *402*, 125881. [[CrossRef](#)]
57. Wang, Q.; Xu, Z.; Jiang, Y.; Lu, J.; Li, H.; Du, X.; Wang, Z. Efficient peroxymonosulfate activation and less metallic leaching through kaolin@MnCo<sub>2</sub>O<sub>4</sub> for bisphenol A degradation in environmental remediation. *Appl. Surf. Sci.* **2022**, *585*, 152705. [[CrossRef](#)]
58. Guan, C.; Jiang, J.; Pang, S.; Luo, C.; Ma, J.; Zhou, Y.; Yang, Y. Oxidation Kinetics of Bromophenols by Nonradical Activation of Peroxydisulfate in the Presence of Carbon Nanotube and Formation of Brominated Polymeric Products. *Environ. Sci. Technol.* **2017**, *51*, 10718–10728. [[CrossRef](#)] [[PubMed](#)]
59. Serna-Galvis, E.A.; Cáceres-Peña, A.C.; Torres-Palma, R.A. Elimination of representative fluoroquinolones, penicillins, and cephalosporins by solar photo-Fenton: Degradation routes, primary transformations, degradation improvement by citric acid addition, and antimicrobial activity evolution. *Environ. Sci. Pollut. Res.* **2020**, *27*, 41381–41393. [[CrossRef](#)] [[PubMed](#)]

**Disclaimer/Publisher's Note:** The statements, opinions and data contained in all publications are solely those of the individual author(s) and contributor(s) and not of MDPI and/or the editor(s). MDPI and/or the editor(s) disclaim responsibility for any injury to people or property resulting from any ideas, methods, instructions or products referred to in the content.